Development 137, 1635-1643 (2010) doi:10.1242/dev.047316

Multispectral four-dimensional imaging reveals that evoked activity modulates peripheral arborization and the selection of plane-polarized targets by sensory neurons

Adèle Faucherre*, Jean-Pierre Baudoin, Jesús Pujol-Martí and Hernán López-Schier*

SUMMARY

The polarity of apical stereocilia endows hair cells with directional excitability, which in turn enables animals to determine the vectorial component of a sound. Neuromasts of the lateral line of aquatic vertebrates harbor two populations of hair cells that are oriented at 180° relative to each other. The resulting sensory-vectorial ambiguity is solved by lateralis afferent neurons that discriminate between hair cells of opposite polarities to innervate only those with the same orientation. How neurons select identically oriented hair cells remains unknown. To gain insight into the mechanism that underlies this selection, we devised a simple method to gather dynamic morphometric information about axonal terminals in toto by four-dimensional imaging. Applying this strategy to the zebrafish allowed us to correlate hair cell orientation to single afferent neurons at subcellular resolution. Here we show that in zebrafish with absent hair cell mechanoreception, lateralis afferents arborize profusely in the periphery, display less stability, and make improper target selections. Central axons, however, show no dynamic changes and establish normal contacts with the Mauthner cell, a characteristic second-order target in the hindbrain. We propose that the hardwired developmental mechanisms that underlie peripheral arborization and target recognition are modulated by evoked hair cell activity. This interplay between intrinsic and extrinsic cues is essential for plane-polarized target selection by lateralis afferent neurons.

KEY WORDS: Hair cells, Planar polarity, Regeneration, Sensory neurons, Deafness, Zebrafish

INTRODUCTION

Sensory perception is a complex process that allows organisms to sample the environment and to react appropriately (Fain, 2003; Hudspeth, 1997). Therefore, sensory dysfunction can be a major handicap that dramatically decreases the quality of life of the affected individual. Deafness, for example, can cause communication problems and may increase the risk of social isolation (Petit et al., 2001; Petit and Richardson, 2009). Sensory systems consist of external sensory receptors that are connected to higher brain areas with cognitive functions via afferent neuronal pathways. Historically, a great emphasis has been placed on the genetic bases of sensory organ innervation during embryonic development. However, most animals spend the overwhelming majority of their lives as adults, when the continuous refinement of organ innervation is not under strict genetic control but is often modulated by extrinsic factors such as sensory activity, disease or pharmacological agents. Sensorineural circuit maintenance, in particular, must converge the intrinsic mechanisms that link cellular identity to target recognition during embryonic development with extrinsic signals that stabilize or destabilize synapses in the adult. This is particularly important for organs with high sensory cell turnover.

The inherent difficulty of studying animals after birth, however, has hampered our understanding of the long-term dynamics of organ innervation. Explanted tissues rarely provide an ideal system to study sensory organs because they perform their main physiological function of transmitting external stimuli to the brain only in their native context. Hearing is a mechanosensory modality that presents a particularly important challenge because inner-ear hair cells and neurons are very difficult to visualize in their natural context even in newborn animals. By contrast, aquatic vertebrates such as fishes and amphibians have a functionally sophisticated but anatomically simple superficial mechanosensory organ called the lateral line (Dambly-Chaudière et al., 2003; Flock, 1971; Ghysen and Dambly-Chaudière, 2004; Ghysen and Dambly-Chaudière, 2007; Lowenstein, 1967). In the zebrafish, each organ of the lateral line contains 20-30 hair cells that are divided into two populations, the stereocilia of which are oriented at 180° relative to each other (López-Schier et al., 2004). These peripheral mechanosensory cells communicate hydromechanic variations around the animal's body to the brain through direct synaptic contact with lateralis afferent neurons (Dijkgraaf, 1962; Gompel et al., 2001). These neurons are bipolar, projecting central and peripheral axons that terminate in ornate arbors (Claas and Münz, 1981; Ghysen and Dambly-Chaudière, 2004). In the lateral line, the spatial distribution of hair cells of different planar polarities changes as organs grow or hair cells die and regenerate (López-Schier and Hudspeth, 2006). Therefore, lateralis sensory neurons must remodel their peripheral axonal arbors accordingly. This implies that cues originating from the hair cells could influence the intrinsic arborization ability of the lateralis neurons, and their selection of plane-polarized targets (Faucherre et al., 2009).

In the present study, we test these hypotheses using the zebrafish lateral line organ, which combines the three-dimensional organization of a sensory receptor with a simple neural component, the dynamics of which can be visualized over long periods and under controlled physiological conditions. We report a comprehensive

Laboratory of Sensory Cell Biology and Organogenesis, Centre de Regulació Genòmica, Doctor Aiguader 88, (08003) Barcelona, Spain.

*Authors for correspondence (adele.faucherre@crg.es; hernan.lopez@crg.es)

Accepted 11 March 2010

study of afferent neuron arborization and plane-polarized target selection using quantitative in toto live imaging and analytical methods in wild-type animals and in specimens with defective hair cell mechanoreception.

MATERIALS AND METHODS

Animals

Zebrafish were maintained under standardized conditions and experiments were conducted in accordance with protocols approved by the PRBB Ethical Committee of Animal Experimentation. Embryos were staged according to Kimmel et al. (Kimmel et al., 1995). The *brn3c:gfp* transgenic line, which expresses GFP in hair cells, was obtained from Herwig Baier (UCSF). HGn39D, *Tg(HuC:Kaede)* and *Tg(islet1:gfp)* have been published previously (Higashijima et al., 2000; Sato et al., 2006).

Morpholino injections

Morpholino oligonucleotides (MOs) were obtained from Gene Tools (Philomath, OR, USA). The sequence of the MO to *cdh23* is 5′-CTCCCGAACCTTCACACCACGACAT-3′ (Sollner et al., 2004). MO (2.5 ng) was co-injected with the HuC:mem-TdTomato construct (10 pg) and transposase (TPase) RNA (10 pg) into one-cell stage embryos. Analysis of the morphants was conducted 4 days after injection.

Labeling and imaging

Immunostainings were performed as described (Faucherre et al., 2009). The primary rabbit anti-Ribeye B antibody was used at 1/100. Cy5-labeled donkey anti-rabbit secondary antibody (Jackson ImmunoResearch) was used at 1/150. We conducted analyses of hair cell orientation, performed vital imaging and screened embryos as described (Faucherre et al., 2009). Wild-type fish, *tmie* mutants and Cdh23 morphants were sorted depending on DiASP incorporation.

Images were acquired with a Leica TCS SPE confocal microscope with a 40× oil-immersion objective or with a Leica TCS SP5 confocal microscope with a 20× dry objective. *z*-stacks were acquired at 0.8 or 0.5 μm intervals, imaging GFP (488 nm excitation, 500-550 nm emission) and TdTomato (532 nm excitation, 570-630 nm emission). Kaede was photoconverted from green to red fluorescence by exposing the larvae to 405 nm light for 2 minutes.

Dextran injections

Dextran (3% in 0.2 M KCl) was dried on a glass slide. To retrogradely label the Mauthner cells, anesthetized fish at 5 days post-fertilization (dpf) were placed on their side in a humidified Petri dish. Using a stereomicroscope, fish were injected with the tip of a tungsten needle (World Precision Instruments, 501316) covered by a minute amount of dried fluorescein-dextran (Invitrogen, D3306) and manually inserted by micromanipulation into the spinal cord at the level of the cloacum. The fish were allowed to recover until 6 dpf and then injected under the same conditions with Alexa 647-dextran (Invitrogen, D22914) and Rhodamine-dextran (Invitrogen, D3308) in the posterior (P9, terminal neuromast) and anterior (SO2, supra-orbital) neuromasts. Animals were selected at 7 dpf for green and red fluorescence in the Mauthner cells and neuromast central projections. They were then mounted on their side in 1% agarose and imaged at the level of the hindbrain using a Leica SPE confocal microscope with a ×40/1.15 ACS APO oil CS objective. Far-red fluorescence of P9 projections was checked with the confocal microscope. Lateromedial *z*-stacks consisted of 0.5 μm-spaced images, starting at the level of lateral line projections and finishing at the medial part of the Mauthner soma. Mean *z* thickness of the stacks was 150 μm (n=6). Three-dimensional (3D) reconstructions and cropping of *z*-stacks were realized with Imaris software (Bitplane).

Four-dimensional (4D) quantification of axonal arbors

We used double-transgenic animals to perform quantitative analyses of axonal arbors in vivo in three dimensions (x=80 μm; y=80 μm; z=20 μm, at 0.5 μm or 0.8 μm intervals) at a rate of one 3D stack every 10 minutes for 1 hour. Digital 4D reconstructions of GFP-positive hair cells and mem-TdTomato afferent neurons were obtained from individual optical sections through the entire extent of the neuromast and the neuronal arbor with the aid of Imaris software. We subsequently quantified changes in arbor complexity by volumetry and kinetics (changes in arbor structure).

Neuronal arbor tracing

Three-dimensional reconstructions of each time point were aligned using the Spot/Correct Drift function of Imaris. Tracing of the neuronal arbor was performed using the FilamentTracer Imaris module. Briefly, the Autopath (no loops) algorithm was used and the starting point was manually selected at the first bifurcation point and assigned as the dendrite beginning point. End points were also manually selected and filaments automatically traced. Final tracing was checked manually and corrected if needed. The process was repeated for every time point.

Four-dimensional rendering

In order to visualize the different positions of a specific tip over time, each terminal point was selected, copied in order to be visible at every time point and one color attributed to each.

Quantification of neurite complexity

Presence

The number of terminal points was counted for each sample at each of the six time points. The average of number of neurites (number of terminal points) was calculated for the wild-type fish, the *tmie* mutants and the Cdh23 morphants.

Stability

Neurite stability was expressed by calculating the percentage of stable neurites (present throughout the six time frames, i.e. for 1 hour) versus the percentage of transient neurites (neurites visible for fewer than six time points). The average was calculated for the wild-type fish, the *tmie* mutants and the Cdh23 morphants.

Persistence

The persistence of the neurites was calculated from the percentage of neurites present for only one, two, three, four, five or all six time frames.

Consistency

We defined consistency as the number of events (growth or retraction) observed for each neurite. ‘Consistent’ refers to a neurite that has neither grown nor retracted over the six time frames. ‘One event’ refers to a neurite that has only grown or only retracted over the six time frames. ‘Two events’ refers to a neurite that completed a sequence of two different movements, i.e. growth followed by retraction or vice versa. Similarly, ‘three events’ refers to a sequence of three different movements; for example, growth followed by retraction followed by growth. To calculate growth and retraction, the position value of a neurite at a specific time point is subtracted from the value of the previous time point. Therefore, positive values correspond to growth and negative values to retraction. Arbitrarily, we decided that significant growth or retraction movements correspond to absolutes of greater than 1.5 μm. Consistency is represented by the percentage of neurites that has achieved a number of events.

Dynamics

At every time point, each terminal point was selected and the distance between this terminal point and the beginning point, following the neuronal path, was obtained with the statistical menu of the filament tracer. Neurites were subdivided into three categories: those exhibiting bulged contacts with hair cells and present throughout the six time frames (bulged); those present throughout the six time frames but without bulged contacts (stables); and transient neurites. The value of the terminal point position at the first time point was normalized to zero and the same value subtracted from the subsequent time points in order to establish the distance traveled by the neurite tip. In the case of transient neurites, the zero position was attributed to the branching point from which the neurite extended.

RESULTS

The structural diversity of lateralis afferent peripheral arbors

To unravel the mechanisms responsible for the selection of plane-polarized hair cells by lateralis afferent neurons, we performed a detailed reconstruction of optically isolated axonal arbors in toto at high spatial resolution. This analysis is straightforward because each

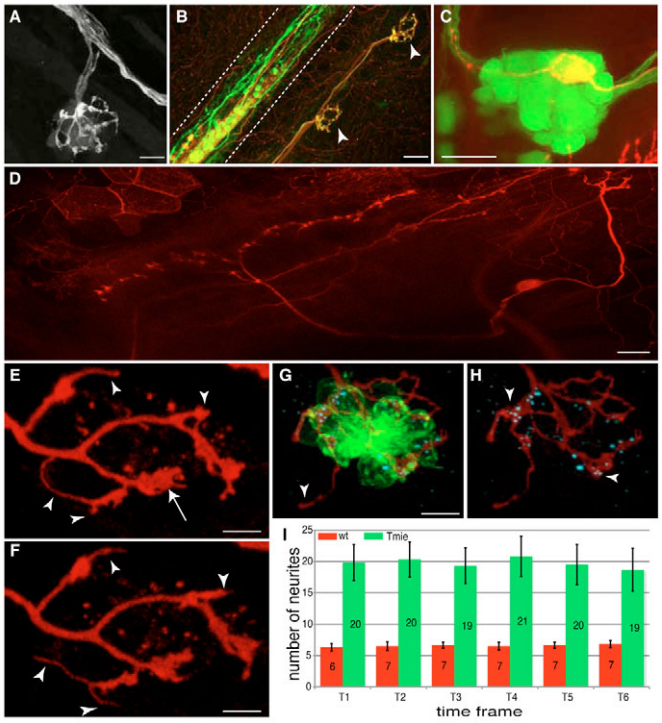

Fig. 1. Central and peripheral projections of lateralis afferent neurons. (**A**) GFP-positive peripheral projections in the HGn39D transgenic zebrafish line. Three afferent neurons projecting to a neuromast are depicted. (**B**) Neuromast innervation in a *HuC:Kaede* and *islet1:gfp* double-transgenic larva after Kaede photoconversion. Green neurons are GFP positive, red neurons are Kaede positive and yellow neurons are GFP/Kaede positive. Neuromasts are innervated by both red and yellow neurons. Arrowheads indicate the neuromasts. Dashed lines delimit the spinal cord. (**C**) Soma of a single TdTomato-positive afferent neuron in a GFP-positive posterior ganglion of an HGn39D transgenic fish. The soma expressing TdTomato is localized in the posterior lateral line ganglion. (**D**) Central projection of a single TdTomato-labeled afferent neuron. Anterior is to the left and posterior to the right. (**E**,**F**) Peripheral projections of a single TdTomato-labeled afferent neuron at two different time frames (10-minute interval). The arrow indicates a bulged extremity, whereas the arrowheads indicate thin and mobile neurites. (**G**,**H**) Anti-Ribeye B immunostaining. The formation of ribbon synapses between the afferent neuron (red) and the hair cells (green) is visualized by the presence of the Ribeye B protein (cyan). Arrowheads indicate (G) a thin neurite that does not contact a hair cell, and (H) bulged neurites containing the Ribeye B protein. (**I**) The average number of neurites present at each time point for wild-type (wt) and *tmie* mutant fish. Error bars represent the s.e.m. Wild type, *n*=6; *tmie*, *n*=6. Scale bars: 10 μm in A,G,H; 20 μm in B-D; 5 μm in E,F.

lateral line organ in the zebrafish larva is innervated by only two or three afferent neurons (Fig. 1A) (Faucherre et al., 2009). Initially, we sought to investigate the elaboration of axonal arbors using UV-mediated photoconversion of single lateralis afferents in *Tg(HuC:Kaede)* (*HuC* is also known as *elavl3* – Zebrafish Information Network) stable transgenic fish, which has been reported to highlight the afferent neurons of the lateral line (Caron et al., 2008). However, we found that in larvae resulting from a cross between the efferent marker *Tg(islet1:gfp)* and *Tg(HuC:Kaede)*, efferent neurons of the lateral line were also labeled by Kaede (Fig. 1B). Thus, we could not unequivocally assign an afferent identity to neurons of the lateral line in *Tg(HuC:Kaede)*.

Instead, we determined afferent neuronal morph by injecting a plasmid encoding HuC:mem-TdTomato, as previously reported (Faucherre et al., 2009). We selected for analysis only those specimens with single red-fluorescent neurons, the soma of which were localized within the lateralis afferent ganglion, which can be marked using the HGn39D transgenic line (Fig. 1C) (Faucherre et al., 2009). Injections were performed in stable *Tg(brn3c:gfp)* (*brn3c* is also known as *pou4f3* – Zebrafish Information Network) eggs to visualize all hair cells with EGFP (Xiao et al., 2005). To reconstruct axonal arbors, we devised a simple method using inexpensive and widely accessible commercial tools.

Our 3D reconstruction of optically isolated neurons showed that lateralis afferents project stereotypic central axons that enter the hindbrain and bifurcate, forming an anterior branch and a posterior branch (Fig. 1D) (Metcalfe et al., 1985). By contrast, peripheral axonal arbors were structurally diverse (Fig. 1E,F), typically forming different types of neurites. Bulged neurites were stably associated with hair cells in what are likely to be synaptic connections, as the bulges adjoined synaptic ribbons as revealed by immunolabeling with an antibody to Ribeye B (Ctbp2l – Zebrafish Information Network) (Fig. 1G,H) (Sidi et al., 2004). Thin neurites were longer and did not always contact hair cells (Fig. 1E-G). One explanation for the diversity of peripheral axon structure is that they are dynamic.

To examine their behavior, we reconstructed peripheral terminals by live imaging at high temporal and spatial resolution. We acquired *z*-stacks of the entire axonal arbor every 10 minutes over a period of 1 hour and subsequently rendered them 3D over time (*n*=6). Arbors were rebuilt by semi-manual tracing of all the filaments at every time point, which allowed us to quantify the behavior of the different neurites (see Table S1 in the supplementary material). This analysis showed that neurites constantly change length and position. On average, neurites grew or retracted at a rate of 100 nm per minute and were capable of extending as much as 5 μm in 10 minutes (Fig. 1E,F). Despite these rapid changes in shape, arbor complexity did not change because the average number of neurites was maintained during the recorded period (Fig. 1I). This is consistent with previous live imaging observations that the rate of neurite sprouting is equivalent to that of pruning (Faucherre et al., 2009). We also found that neurite sprouting occurred by interstitial branching and that pruning occurred through retraction, as we never observed neurite shedding or degeneration. We conclude that the structural diversity of afferent peripheral arbors results from a very active process of neurite production, extension and retraction.

Peripheral arborization is modulated by hair cell activity

The observation that neuron sprouting activity is lower in quiescent neuromasts than in those undergoing regeneration suggests that peripheral arbors restructure in response to cues from the sensory epithelium (Faucherre et al., 2009). We asked whether these cues originate from hair-cell activity by taking advantage of a zebrafish strain with a loss-of-function mutation in *tmie*, the ortholog of the mammalian deafness gene transmembrane inner ear. Homozygous *tmie* mutant zebrafish are viable and fertile, but profoundly deaf due to defects in hair cell mechanoreception (Gleason et al., 2009).

We scatter-labeled lateralis afferents by injecting HuC:mem-TdTomato DNA into wild-type and *tmie* mutant eggs that also carried the *Tg(brn3c:gfp)* transgene. Again, axons were identified as afferent when they could be traced to a soma located in the postotic ganglion. We acquired 4D images and found that in every case the peripheral arbors were significantly more complex in *tmie*

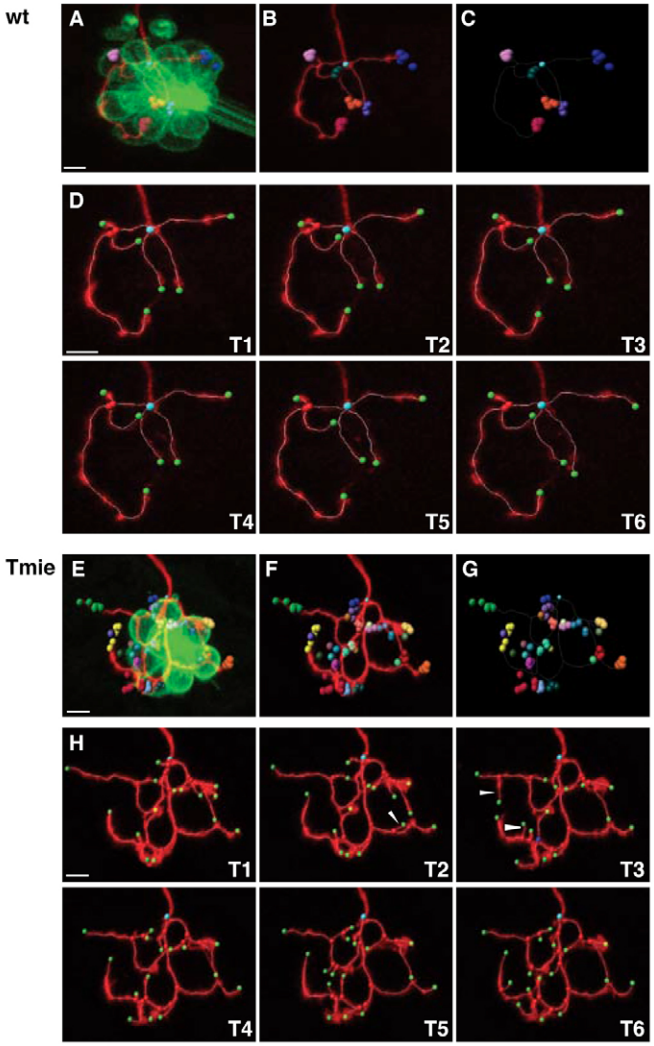

Fig. 2. Four-dimensional reconstruction of a single labeled afferent neuron. (A-G) Four-dimensional representations of an afferent neuron in wild-type (A-C) and *tmie* mutant (E-G) fish. (**A**,**E**) mem-TdTomato-labeled neuron contacting the GFP-expressing hair cells. The terminal point of each neuron has been plotted with a different color. For each terminal point (i.e. for each color) positions have been plotted over time, every 10 minutes for 1 hour. (**B**,**F**) Same as A,E but without the hair cells. (**C**,**G**) Same as B,F but with only the dots representing the terminal point. The unique cyan dot indicates the beginning point of the neuronal arbor. The white frame corresponds to the neuronal arbor reconstruction of the first time frame. (**D**,**H**) Maximal projections and neuronal arbor reconstruction of the same neuron over time. Images T1-T6 were taken every 10 minutes for 1 hour. Beginning point is in cyan, terminal points are in green, branching points are in red, and special branching points (multiple bifurcations) are in blue. Arrowheads indicate examples of transient neurites. Scale bars: 5 μm.

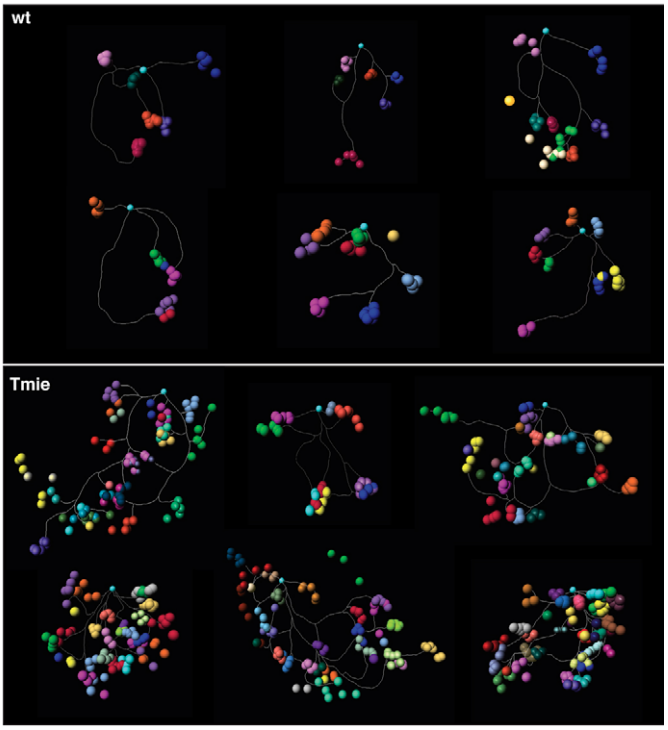

Fig. 3. Four-dimensional representations of a single labeled afferent neuron. Four-dimensional representations of single labeled afferent neuron in six wild-type (above) and *tmie* mutant (below) fish. The terminal point of each neuron has been plotted with a different color. For each terminal point (i.e. for each color) positions have been plotted over time, every 10 minutes for 1 hour.

fish (n=6) than in wild-type controls (n=6) at 7 dpf. We quantified arbor complexity by adopting different strategies. We assigned numerical complexity by counting the total number of neurite termini per arbor. For dynamic complexity, we generated a visual representation of the arbors by placing a colored dot on each neurite terminus. Subsequently, the position of each terminus was tracked in 3D space every 10 minutes for 1 hour. Termini were assigned a different color at each of the six time points that divided the whole recording period (Figs 2 and 3; see Movies 1-4 in the supplementary material). Comparison of the numerical and dynamic complexity between wild-type and *tmie* animals indicated that the group of mutants had, on average, a 2-fold increase in the number of neurites at each time point (Fig. 1I and see Fig. S1A in the supplementary material). For example, the *tmie* mutant in Fig. 2 had 16 neurites at the first time frame, whereas wild-type fish displayed only six branches at the same time point.

Next, we compared arbor stability by counting the number of neurites present throughout the six time points imaged (stable neurites) and also those that were observed in only one to five of the time frames (transient neurites). In *tmie* mutants 40% of the neurites were transient, significantly higher than the 12% found in wild-type specimens (P<0.01) (Fig. 4A and see Fig. S1B in the supplementary material). We next counted the number of neurites that were visible during one to five of the time frames and defined ‘persistence’ as the ability of a neurite to remain present during a defined period. This analysis revealed that the majority (88%) of wild-type neurites was present throughout the whole recorded period, whereas only 59% of the neurites in *tmie* fish were present during all six time frames. We found that 14% of *tmie* neurites were present for only one time frame, compared with 7% in the wild type (Fig. 4B). Therefore, neurites of *tmie* mutants were less persistent.

We then probed wild-type and *tmie* neurites for their ‘consistency’. We defined consistency as the persistence of their behavior (Fig. 4C). For example, neurites that have neither grown

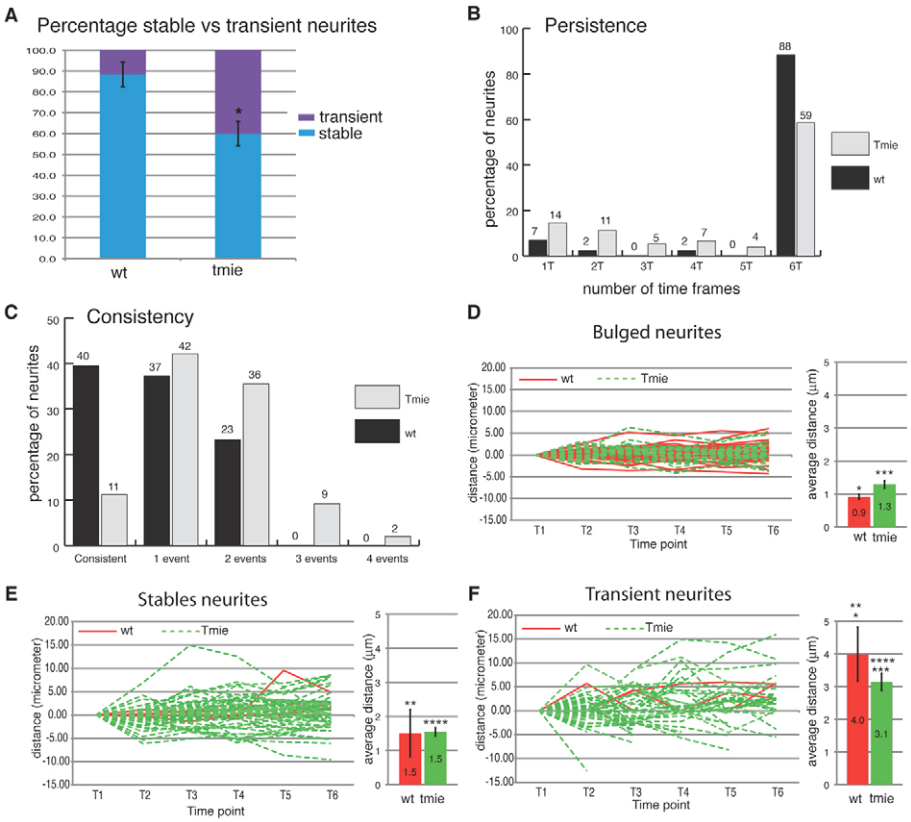

Fig. 4. Quantitative analysis of neurite dynamics. (**A**) Average of stable (present throughout the six time frames) versus transient (present in fewer than six time frames) neurites in wild-type and *tmie* mutant fish. Error bars represent the s.e.m. *, $P<0.01$. (**B**) Neurite persistence. Persistence of neurites was calculated from the percentage of neurites present for only one, two, three, four, five or all six time frames. (**C**) Neurite consistency. 'Consistent' refers to a neurite that has neither grown nor retracted over the six time frames. 'One event' refers to a neurite that has only grown or retracted over the six time frames. 'Two events' refers to a neurite that completed a sequence of two counter movements, i.e. growth followed by retraction or vice versa. Similarly, 'three events' refers to a sequence of three counter movements. (**D-F**) Dynamics of neurites tips. The value of the terminal point position at the first time point was normalized to zero and the same value was subtracted from the subsequent time points in order to establish the distance traveled by the neurite tip. On the right of each graph is shown the average distance (µm) traveled by each type of neurite during one time frame. Stable neurites lack a bulged extremity but are present throughout the six time frames. (D) Dynamics of bulged neurites. (E) Dynamics of stable non-bulged neurites. (F) Dynamics of transient neurites. Red lines, wild type; dashed green lines, *tmie*. Error bars represent s.e.m. *, ***, ****, $P<0.01$; **, $P<0.1$ for pairs indicated by number of asterisks; wild type, $n=6$; *tmie*, $n=6$.

nor retracted for the whole recorded period were classified as highly consistent, whereas those that performed a sequence of counter behaviors (e.g. growth then retraction) defined a lower degree of consistency. In *tmie* mutants, only 11% of neurites were absolutely consistent, whereas 42% grew or retracted, and 36%, 9% and 2% performed a sequence of two, three or four counter events, respectively. By comparison, in wild-type fish the respective values were 40%, 37%, 23%, 0% and 0%. Thus, neurites in *tmie* mutants are less consistent.

Finally, we measured the distance traveled by each neurite from the first time point. For a more accurate analysis, we subdivided them into three categories: bulged neurites that were present throughout the six time frames (bulged); neurites that were present throughout the six time frames but without bulging (stable); and neurites of low persistence (transient). Wild-type and mutant transient neurites traversed significantly longer distances during one time point than stable and bulged neurites (Fig. 4D-F).

To confirm that the observed effects were caused by the loss of hair cell activity, we applied the same strategy to animals injected with a morpholino (MO) against *cadherin 23* (*cdh23*). Cdh23 morphants phenocopy the *sputnik* zebrafish strain, which bear a mutation in *cdh23* that also causes deafness and lack of mechanoreception due to absent tip links (Sollner et al., 2004). The study was conducted at 4 dpf for maximal MO efficiency. Similar to *tmie* mutants, Cdh23 morphants showed more complex peripheral arbors than control fish. On average, we observed a 1.7-fold increase in the number of neurites, with 46% of neurites being transient in morphants versus 17% in controls. We also found that neurites were less persistent and less consistent in Cdh23 morphants (controls, $n=3$; *cdh23* MO, $n=3$) (see Fig. S2 and Table S2 in the supplementary material). From these results, we conclude that the complexity of afferent neuron peripheral arbors is influenced by the sensory epithelium, and that arbor stability depends on evoked hair cell activity.

Central axons appear normal in profoundly deaf zebrafish

We next asked whether profound deafness would also influence neuron central axons. We assessed lateralis afferent central somatotopy and contacts with the Mauthner cell, a characteristic second-order target in the posterior hindbrain (Kimmel et al., 1982; Metcalfe et al., 1985). The lateral dendrite of the Mauthner cell has

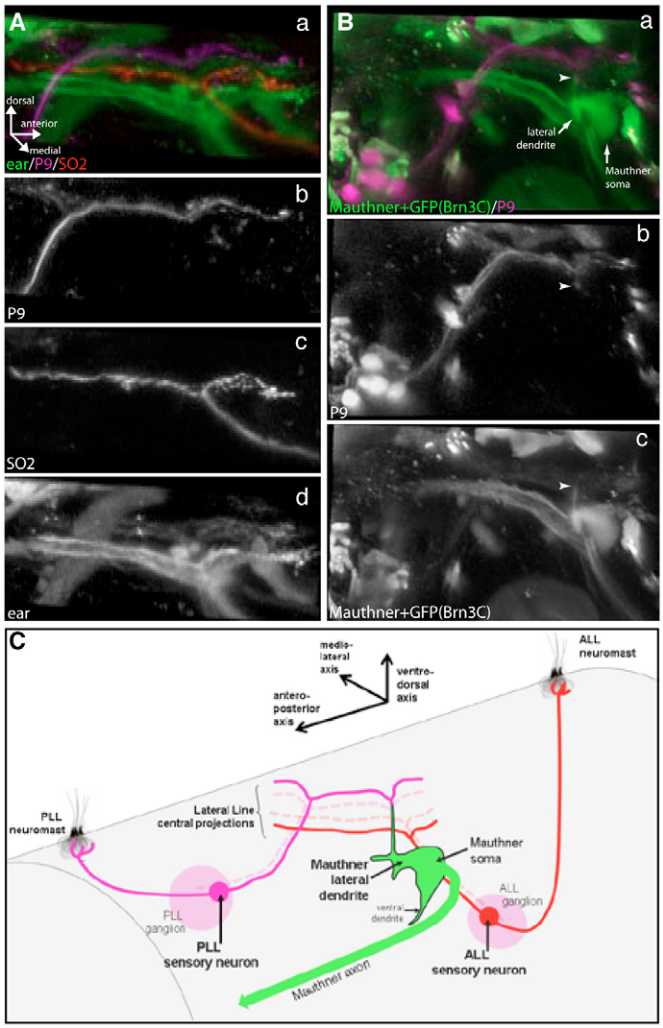

Fig. 5. Central projections of first-order lateral line sensory neurons in *tmie* mutants. Central somatotopy and targeting of the Mauthner cell are conserved in *tmie* mutants. (**Aa-d**) Fluorescent dextran injections in *tmie*$^{-/-}$ *brn3c:gfp* transgenic fish showing somatotopy of first-order lateral line sensory neuron projections coming from posterior (b) and anterior (c) neuromasts. Projections coming from P9 (PLL) neuromasts (b; Alexa 647-dextran) and SO2 (ALL) neuromasts (c; Rhodamine-dextran) project in a dorsoventral manner (a) in the hindbrain. (d) Projections coming from the ear (Brn3c:GFP). (**Ba-c**) Fluorescent dextran injections in *tmie*$^{-/-}$ *brn3c:gfp* transgenic fish showing central targeting of the Mauthner lateral dendrite by posterior and anterior lateral line projections (a). Projections coming from the P9 (PLL) neuromast (b; Alexa 647-dextran) connect (arrowheads) to the lateral-most portion of the Mauthner cell lateral dendrite (c; fluorescein-dextran), which extends ventrodorsally. (**C**) Scheme (not to scale) depicting the central somatotopy of the first-order lateral line sensory neuron projections, and their targeting of the Mauthner cell lateral dendrite. In *tmie* fish, the anteroposterior axis of the lateral line neuromast projects onto the ventrodorsal axis of the Mauthner lateral dendrite dorsal projection, as in wild-type fish. ALL, anterior lateral line; PLL, posterior lateral line.

a dorsal projection at its lateral tip that is the target of the lateralis afferent projections (Fig. 5C). To reveal the Mauthner cell, we injected green fluorescent dextran into the spinal cord of *tmie* mutant larva. This dye is incorporated into the axon of the Mauthner cell and retrogradely spreads through the entire cell, including its two dendrites. We also injected magenta (in a terminal neuromast of the posterior lateral line) and red (in a supra-orbital neuromast of the anterior lateral line) fluorescent dextran to retrogradely label the afferent neurons that innervate these neuromasts (Sapède et al., 2005).

Tracing afferent neurons to the hindbrain showed that their central organization was unaffected in *tmie* mutants (n=7) (Fig. 5B and see Movie 5 in the supplementary material). In addition, the central projections from anterior and posterior neuromast afferents extended normally and were correctly placed along the somatotopic axis in the hindbrain (Fig. 5A). We observed that posterior and anterior lateral line central axons made contacts with the lateral dendrite of the Mauthner cell at the level of the dorsal projection (Fig. 5Ba and see Movie 5 in the supplementary material) as in wild-type controls (data not shown). In addition, live imaging at resolutions identical to those applied to peripheral arbors revealed no dynamic changes in the neuron central arbors (data not shown). These results show that the lack of evoked hair cell activity has no major impact on the central axonal organization of lateralis neurons.

Afferent neurons cannot discriminate target orientation in the absence of hair cell mechanoreception

Because deafness dramatically affected peripheral arborization, we asked whether evoked hair cell activity plays any role in the selection of plane-polarized targets by the afferent neurons. We scatter-labeled neurons and revealed hair cell orientation by labeling their apical stereocilia with fluorescent phalloidin (Fig. 6A,B). Homozygous *tmie* mutant fish develop hair cells with normal planar cell polarity (Fig. 6B) (Gleason et al., 2009). In wild-type fish, 88% of the bulged neurites associated exclusively with hair cells of a single polarity (n=17), significantly higher than the 38% found in *tmie* mutants (n=21) (Fig. 6C). In *tmie* mutants, 62% of bulged neurites were associated with hair cells of both polarities, an occurrence seen much less frequently in wild-type animals (12%). In *tmie* and wild-type specimens, bulged neurites established synapses with hair cells as revealed by the localized concentration of Ribeye B puncta (Fig. 6D-I) (wild type, n=6; *tmie*, n=7). Furthermore, several thin neurites also appeared to establish synapses with hair cells (Fig. 6J-L).

Mechanotransmission between a hair cell and its afferent neurons is mediated by glutamate release from the hair cell, which activates AMPA receptors in the neurons (Bailey and Sewell, 2000). To further probe hair cell polarity discrimination by the neurons, we attempted a pharmacological approach using glutamate receptor agonists and antagonists. We treated fish with CNQX (a competitive AMPA/kainate glutamate receptor antagonist), domoic acid (a potent agonist of AMPA/kainate glutamate receptors), kanaic acid (an agonist of the kainate/glutamate receptor), maleate (a non-competitive NMDA receptor antagonist) and cyclothiazide (an allosteric inhibitor of AMPA receptor desensitization that alters receptor gating). None of these drugs produced a phenotype in fish that was consistent with synaptic inhibition (data not shown), suggesting that they did not effectively impact their target in our in vivo experimental set-up. We also tried to electrically silence neuronal activity by expressing the inward-rectifier potassium ion channel Kir2.1 in lateralis afferents (Hua et al., 2005). Although Kir2.1 expression in afferent neurons did not affect their development, it had a profound impact on neuritogenesis and also led to late-onset neuronal degeneration (data not shown). Thus, this approach was also unsuccessful. In spite of this, we interpret our

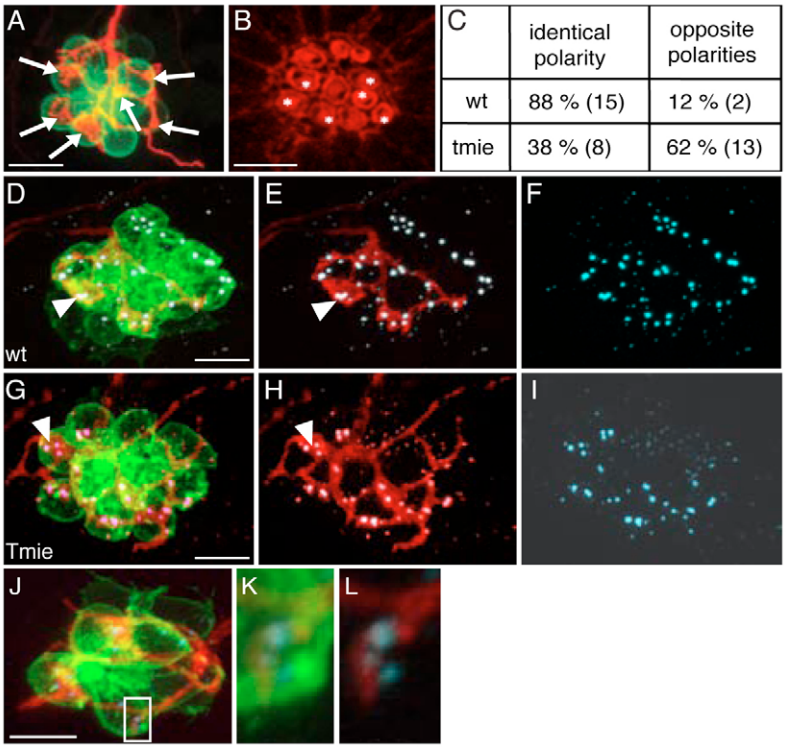

Fig. 6. Afferent neurons from *tmie* mutants are not strict polarity selectors. (**A-C**) Analysis of polarity-specific innervation in HuC:mem-TdTomato-injected *brn3c:gfp tmie* mutants. (A) Maximal projection and (B) phalloidin staining of a neuromast innervated by a single labeled afferent neuron in a *tmie* mutant. Arrows in A indicate bulged neurites establishing contacts with the hair cells. Asterisks in B indicate the innervated hair cells. (C) The percentage of contacts established between an afferent neuron and hair cells of identical polarity or hair cells of two opposing polarities. The numbers in brackets indicate the number of neuromasts (wild type, *n*=17; *tmie*, *n*=21). (**D-L**) Immunodetection of ribbon synapses in wild type (D-F) and *tmie* (G-L) fish using the Ribeye B antibody (cyan). Bulged contacts of afferent neurons expressing TdTomato (red) with hair cells (green) are associated with the presence of synapses in wild type (D-F) and *tmie* (G-I) fish (arrowheads indicate an example in each case). Thin neurites can also form synapses with hair cells as shown by the presence of Ribeye B staining in the neuromast of a *tmie* mutant (J-L). The boxed area in J is magnified in K,L. Scale bars: 10 μm in A,D,G,J; 5 μm in B.

results from the profoundly deaf *tmie* mutants as a clear indication that evoked hair cell activity is necessary for afferent neurons to correctly select identically oriented targets.

DISCUSSION

Previous studies have established that the stimulus polarity problem posed by the dual planar polarization of hair cells in the lateral line system is solved by the afferent neurons through orientation-based selection of targets, but the mechanisms that govern the ability of the neuron to perform this selection have remained unknown. Here, we report a comprehensive study of the elaboration and maintenance of afferent neuron axonal arbors and of plane-polarized target selection using profoundly deaf zebrafish and in toto quantitative live imaging.

Four-dimensional analysis of axonal arbors

Investigations of neuronal arborization and target selection are motivated by an interest in the mechanisms that control sensory circuit homeostasis, the properties of which determine the quality of the information transfer process. The acusticolateralis sensory systems that comprise the inner ear and lateral line in vertebrates rely on the planar polarization of their external sensory elements, called hair cells, for coherent information transfer. This organization allows animals to detect and interpret the direction of propagation of a sound. Because hair cells display their characteristic planar polarization only within an intact epithelium, the circuits that use this architectural property of the receptors for sensory transduction cannot currently be studied in vitro, necessitating in toto experimental paradigms. The generation of transgenic animals to label neurons and target cells for multispectral live imaging facilitates computer-assisted image analysis. Given the complexity and inaccessibility of the mammalian nervous system, however, animal models with simpler circuits and accessible neurons provide an opportunity for the accurate reconstruction of sensorineural circuits. Following this rationale, we employed the lateral line of the zebrafish to better understand the mechanisms that underlie the selection of plane-polarized targets by sensory neurons.

We designed a strategy to acquire 4D metric data and to explore how lateralis afferent neurons elaborate their axonal arbors and select synaptic targets in their natural context. Several sophisticated methods have been developed to determine neuronal arborization in two and three dimensions, but they are usually based on custom-made software applications that require a substantial knowledge of programming. This has impeded their generalized use. Therefore, we sought to build a framework to analyze neuron axonal complexity and dynamics using a simple protocol and a commercially available software package with which we were able to study neuronal arbors in detail in four dimensions. Often, neural circuits are characterized from their statistical properties by pooling data from multiple animals and from static images. This can be problematic when a good correspondence between individual samples is lacking, as we have found for the neuron peripheral arbors. Therefore, we employed 4D imaging of individual neurons to show that they project peripheral arbors that are structurally very diverse and that derive from active neurite production, extension and retraction.

An additional aim of our work was to provide interactive 3D representations of the peripheral arbors to allow the viewer to independently assess and interpret our data from free angles. We complement this by providing the raw data of our in vivo neuronal measurements (see Tables S1 and S2 in the supplementary material) that should also allow researchers to easily compare them with any newly generated data. Finally, our strategy offers the advantage of being easily complemented by various experimental manipulations. It could form the bases of further studies of neuronal behavior; for example, during chronic pharmacological treatments or during organ growth and repair.

Peripheral arborization is influenced by evoked hair cell activity

What controls neuronal arborization? We found that the formation of a coarse projection map begins with the intrinsic capacity of the neurons to access the target areas and arborize their central and peripheral axons. At this scale, the process appears independent of hair cell activity because profound deafness did not affect central somatotopy between lateral line branches, or targeting of the Mauthner cell and the superficial neuromasts. However, at later stages, peripheral arbors were more complex in animals that lacked mechanoreception. Deafness also rendered neurites less persistent and consistent. Therefore, our results indicate that the intrinsic developmental mechanisms that underlie axonal arborization are modulated by extrinsic cues that depend on hair cell evoked activity.

How can evoked activity affect peripheral arbor complexity and dynamics? One possibility is that productive synaptic contacts between hair cells and neurons decrease neuron sprouting activity in a manner reminiscent of neuronal homeostasis (Sullivan and de Sa, 2006; Turrigiano and Nelson, 2000). We currently do not know the mechanisms used by hair cells to control peripheral arbor dynamics, other than that it depends on the evoked release of glutamate by hair cells. However, information from other systems suggests that calcium homeostasis might be part of the process (Schwartz et al., 2009). Our quantitative imaging approach combined with the generation of tools for controlled gene expression in hair cells and neurons will soon permit a molecular interrogation of this process in the lateral line of the zebrafish (Scott and Baier, 2009).

Plane-polarized target selection

An important issue in the investigation of neuronal selectivity of targets is the definition of synaptic contacts. We have previously shown that bulged neurites demonstrate contact stability between afferent neurons and hair cells. Here we show that bulged termini are juxtaposed to Ribeye B clustering in hair cells. Thin neurites are highly dynamic and show exploratory behavior, probing hair cells to identify a target. Neurons might need to form synaptic contacts in order to probe the peripheral target, which would require the assembly of the ribbon synapses that depend on Ribeye B accumulation. This might explain why we also detect some Ribeye B puncta adjacent to the tip of several thin neurites (Fig. 6). However, some of these exploratory synapses will disassemble if the selection is incorrect. Bulges would form only after selections were correct, leading to contact stabilization. The higher number of bulged neurites that were associated with hair cells in *tmie* mutants indicates that loss of hair cell activity promotes synaptic stabilization.

Deaf animals showed an increase in peripheral arbor complexity that we interpreted as a sign of dysregulation that could extend to target selectivity. Previous work has ruled out a role of afferent neurons in determining the orientation of hair cells, concluding that afferent neurons detect hair cell polarity to form synapses only to those with identical orientation. However, the cues that allow neurons to recognize hair cell planar polarization have remained unknown (Faucherre et al., 2009; Nagiel et al., 2008). How is this selection achieved? We previously suggested that lateralis afferents use an activity-dependent process to select targets based on their orientation, but it remains possible that a neuron and identically oriented hair cells are matched by an intrinsic molecular code (Faucherre et al., 2009). Although there is no direct evidence of molecular differences that discriminate between neurons and hair cells of a given planar orientation, a recent report supports the chemoaffinity hypothesis based on an apparent absence of differences in target selectivity between normal and deaf animals (Nagiel et al., 2009). Unambiguous identification of the contacts made by bulged endings with hair cells is not always possible using single focal sections. Also, static images that provide a snapshot of a highly dynamic process cannot discriminate between transient and stable associations between neurons and hair cells, and characterizing neuronal behavior by pooling data from multiple animals is prone to averaging (Nagiel et al., 2009). Our high-resolution 3D live imaging of several individual neurons, however, overcomes these limitations with the added advantage that the finer details of neuronal behavior and target selectivity become evident. By rotating the 3D renderings, we could clearly define all neurite types and, in particular, the bulged neurites that stably associated with hair cells. In addition to our more detailed visualization, we independently assessed synaptic contacts by Ribeye B clustering at ribbon synapses.

Taking into account this collective evidence, we do not favor a chemoaffinity code mechanism for two reasons. First, chemoaffinity assumes molecular asymmetries between hair cells of opposite orientations and also molecular differences within the afferent neuronal population, for which there is no evidence (López-Schier and Hudspeth, 2006). Second, if molecular coding governed synaptic partnership, the selection of targets by the neurons should not be altered by a lack of evoked activity. Our testing of this hypothesis using *tmie* mutants and Cdh23 morphants showed that target selectivity is disrupted by profound deafness. We interpret these results as good evidence in support of the conclusion that plane-polarized target selection by sensory neurons relies on evoked hair cell activity. A likely explanation for the differing conclusions is differences in the experimental approaches.

How would activity influence the neuron's choice of synaptic partners? We have previously suggested that during the early stages of peripheral innervation, lateralis afferents have a choice between just two targets because neuromasts first develop a single pair of hair cells with opposite orientation (Faucherre et al., 2009). Initial stochastic contacts between neurons and hair cells would be refined by an activity-dependent mechanism that stabilizes a one-to-one synaptic connection between each neuron and only one of the sibling hair cells. Subsequently, as hair cells of opposite polarities continue to appear sequentially and in pairs, afferents would again choose a new target between only two possibilities. An activity-dependent mechanism would instruct each neuron to form synapses only with hair cells that are polarized along the same vector as the neuron's first target using, as a cue, their simultaneous release of glutamate. In this scenario, peripheral axonal arbors would act as coincidence detectors. Does this imply that there are no asymmetries in the system? We believe that this should not necessarily be the case. However, we hypothesize that if there were any asymmetries, these would be activity based.

Although combinatorial molecular coding remains a possibility, our results do not support chemoaffinity as the sole mechanism that governs the choice of synaptic partners in the lateral line. In the future, it would be interesting to test the impact of hair cell planar polarity defects on neuronal behavior.

Acknowledgements

We thank C. B. Chien for the Tol2 kit and T. Nicolson for the Ribeye B antibody; the ALMU staff for advice on microscopy; and S. Desbordes and all members of our research group for encouragement and discussions. This research was supported by institutional funds from the CRG and by a grant from the European Research Council (ERC-2007-StG SENSORINEURAL). A.F. was supported by an Intra-European Marie Curie fellowship from the European

Union. J.-P.B. was supported by a fellowship of the Fondation pour la Recherche Médicale of France. J.P.-M. is an FPI fellow and H.L.-S. is a Ramón y Cajal Investigator of the Ministerio de Ciencia e Innovación of Spain.

Competing interests statement
The authors declare no competing financial interests.

Author contributions
A.F. and H.L.-S. designed the project; A.F., J.-P.B. and J.P.-M. performed the experiments. All authors analyzed the data, wrote, read and approved the manuscript.

Supplementary material
Supplementary material for this article is available at
http://dev.biologists.org/lookup/suppl/doi:10.1242/dev.047316/-/DC1

References

Bailey, G. P. and Sewell, W. F. (2000). Contribution of glutamate receptors to spontaneous and stimulus-evoked discharge in afferent fibers innervating hair cells of the Xenopus lateral line organ. *Hear Res.* **144**, 8-20.
Caron, S. J., Prober, D., Choy, M. and Schier, A. F. (2008). In vivo birthdating by BAPTISM reveals that trigeminal sensory neuron diversity depends on early neurogenesis. *Development* **135**, 3259-3269.
Claas, B. and Münz, H. (1981). Projection of lateral line afferents in a teleost's brain. *Neurosci. Lett.* **23**, 287-290.
Dambly-Chaudière, C., Sapède, D., Soubiran, F., Decorde, K., Gompel, N. and Ghysen, A. (2003). The lateral line of zebrafish: a model system for the analysis of morphogenesis and neural development in vertebrates. *Biol. Cell* **95**, 579-587.
Dijkgraaf, S. (1962). The functioning and significance of the lateral line organs. *Biol. Rev.* **38**, 51-105.
Fain, G. L. (2003). *Sensory Transduction.* Massachusetts: Sinauer Associates.
Faucherre, A., Pujol-Martí, J., Kawakami, K. and López-Schier, H. (2009). Afferent neurons of the zebrafish lateral line are strict selectors of hair-cell orientation. *PLoS ONE* **4**, e4477.
Flock, Å. (1971). The lateral line organ mechanoreceptors. In *Fish Physiology*, vol. 5 (ed. W. S. Hoar and D. J. Randall), pp. 241-264. New York: Academic Press.
Ghysen, A. and Dambly-Chaudière, C. (2004). Development of the zebrafish lateral line. *Curr. Opin. Neurobiol.* **14**, 67-73.
Ghysen, A. and Dambly-Chaudière, C. (2007). The lateral line microcosmos. *Genes Dev.* **21**, 2118-2130.
Gleason, M. R., Nagiel, A., Jamet, S., Vologodskaia, M., López-Schier, H. and Hudspeth, A. J. (2009). The transmembrane inner ear (Tmie) protein is essential for normal hearing and balance in the zebrafish. *Proc. Natl. Acad. Sci. USA* **106**, 21347-21352.
Gompel, N., Cubedo, N., Thisse, C., Thisse, B., Dambly-Chaudière, C. and Ghysen, A. (2001). Pattern formation in the lateral line of zebrafish. *Mech. Dev.* **105**, 69-77.
Higashijima, S., Hotta, Y. and Okamoto, H. (2000). Visualization of cranial motor neurons in live transgenic zebrafish expressing green fluorescent protein under the control of the islet-1 promoter/enhancer. *J. Neurosci.* **20**, 206-218.
Hua, J. Y., Smear, M. C., Baier, H. and Smith, S. J. (2005). Regulation of axon growth in vivo by activity-based competition. *Nature* **434**, 1022-1026.
Hudspeth, A. J. (1997). How hearing happens. *Neuron* **19**, 947-950.
Kimmel, C. B., Powell, S. L. and Metcalfe, W. K. (1982). Brain neurons which project to the spinal cord in young larvae of the zebrafish. *J. Comp. Neurol.* **205**, 112-127.
Kimmel, C. B., Ballard, W. W., Kimmel, S. R., Ullmann, B. and Schilling, T. F. (1995). Stages of embryonic development of the zebrafish. *Dev. Dyn.* **203**, 253-310.
López-Schier, H. and Hudspeth, A. J. (2006). A two-step mechanism underlies the planar polarization of regenerating sensory hair cells. *Proc. Natl. Acad. Sci. USA* **103**, 18615-18620.
López-Schier, H., Starr, C. J., Kappler, J. A., Kollmar, R. and Hudspeth, A. J. (2004). Directional cell migration establishes the axes of planar polarity in the posterior lateral-line organ of the zebrafish. *Dev. Cell* **7**, 401-412.
Lowenstein, O. (1967). Lateral line detectors. In *Lateral Line Detectors* (ed. P. Cahn). Bloomington: Indiana University Press.
Metcalfe, W. K., Kimmel, C. B. and Schabtach, E. (1985). Anatomy of the posterior lateral line system in young larvae of the zebrafish. *J. Comp. Neurol.* **233**, 377-389.
Nagiel, A., Andor-Ardó, D. and Hudspeth, A. J. (2008). Specificity of afferent synapses onto plane-polarized hair cells in the posterior lateral line of the zebrafish. *J. Neurosci.* **28**, 8442-8453.
Nagiel, A., Patel, S. H., Andor-Ardó, D. and Hudspeth, A. J. (2009). Activity-independent specification of synaptic targets in the posterior lateral line of the larval zebrafish. *Proc. Natl. Acad. Sci. USA* **106**, 21948-21953.
Petit, C. and Richardson, G. P. (2009). Linking genes underlying deafness to hair-bundle development and function. *Nat. Neurosci.* **12**, 703-710.
Petit, C., Levilliers, J. and Hardelin, J. P. (2001). Molecular genetics of hearing loss. *Annu. Rev. Genet.* **35**, 589-646.
Sapède, D., Rossel, M., Dambly-Chaudière, C. and Ghysen, A. (2005). Role of SDF1 chemokine in the development of lateral line efferent and facial motor neurons. *Proc. Natl. Acad. Sci. USA* **102**, 1714-1718.
Sato, T., Takahoko, M. and Okamoto, H. (2006). HuC:Kaede, a useful tool to label neural morphologies in networks in vivo. *Genesis* **44**, 136-142.
Schwartz, N., Schohl, A. and Ruthazer, E. S. (2009). Neural activity regulates synaptic properties and dendritic structure in vivo through calcineurin/NFAT signaling. *Neuron* **62**, 655-669.
Scott, E. K. and Baier, H. (2009). The cellular architecture of the larval zebrafish tectum, as revealed by gal4 enhancer trap lines. *Front. Neural Circuits* **3**, 13.
Sidi, S., Busch-Nentwich, E., Friedrich, R., Schoenberger, U. and Nicolson, T. (2004). gemini encodes a zebrafish L-type calcium channel that localizes at sensory hair cell ribbon synapses. *J. Neurosci.* **24**, 4213-4223.
Sollner, C., Rauch, G. J., Siemens, J., Geisler, R., Schuster, S. C., Müller, U. and Nicolson, T. (2004). Mutations in cadherin 23 affect tip links in zebrafish sensory hair cells. *Nature* **428**, 955-959.
Sullivan, T. J. and de Sa, V. R. (2006). Homeostatic synaptic scaling in self-organizing maps. *Neural Netw.* **19**, 734-743.
Turrigiano, G. G. and Nelson, S. B. (2000). Hebb and homeostasis in neuronal plasticity. *Curr. Opin. Neurobiol.* **10**, 358-364.
Xiao, T., Roeser, T., Staub, W. and Baier, H. (2005). A GFP-based genetic screen reveals mutations that disrupt the architecture of the zebrafish retinotectal projection. *Development* **132**, 2955-2967.